Applied Surface Science 533 (2020) 147483

Contents lists available at ScienceDirect

Applied Surface Science

journal homepage: www.elsevier.com/locate/apsusc

Pyrolyzed pencil graphite coated cellulose paper as an interlayer: An effective approach for high-performance lithium-sulfur battery

Poonam Rani[1], Krishna S. Kumar[1], Anil D. Pathak, Chandra S. Sharma*

Creative & Advanced Research Based On Nanomaterials (CARBON) Laboratory, Department of Chemical Engineering, Indian Institute of Technology Hyderabad, Kandi, Telangana, India

ARTICLE INFO

Keywords:
Pencil graphite
Cellulose filter paper
Interlayer
Polysulfide
Lithium-sulfur battery

ABSTRACT

Lithium-sulfur (Li-S) battery is next generation battery technology but it's commercialization is obstructed primarily due to the shuttling effect of lithium polysulfides (LiPSs). Herein, we report an effective approach using pencil coated pyrolyzed cellulose filter paper as an interlayer to suppress the LiPSs dissolution into the electrolyte and thus allowing effective utilization of active sulfur cathode. Here, the binder clay particles (mainly SiO_2) of pencil graphite facilitate the adsorption of LiPSs, whereas graphite increases the electrical conductivity and acts as a physical barrier to LiPSs. To investigate further, we utilize three different grades of pencil (4B, HB, 5H) which vary in terms of clay (SiO_2) composition. It is observed that the HB pencil coated interlayer has the right balance of silica and graphite, which results in an impressive initial capacity of 1352 and 995 mAh g^{-1} at the current density of 0.1 and 0.5 A g^{-1}, respectively. The cell exhibit high cycling stability of 900 mAh g^{-1} at 1 A g^{-1} (3.0 C) for 350 cycles with a slow capacity decay of 0.07% per cycle. The phenomenon of LiPSs adsorption is further understood using post-cycling analysis, H-cell adsorption testing, and shuttle factor calculation for the development of commercial Li-S batteries.

1. Introduction

Lithium-sulfur (Li–S) battery is presently considered as one of the most promising candidate to replace conventional lithium-ion battery due to the high theoretical specific capacity (1675 mAh g^{-1}) and specific energy density (2500 Wh kg^{-1}) of sulfur cathode [1]. In addition, sulfur is one of the most abundant element on the Earth besides being environment-friendly, low cost, and moreover, meets all the requirements of renewable and clean energy [2]. Even though sulfur has innumerable benefits, commercialization of Li-S battery is challenging because of dissolution of higher-order polysulfide (Li_2S_x, $4 < x \leq 8$) in an organic electrolyte and its poor conductivity (i.e. 5×10^{-30} S cm^{-1}) [3], which leads to low columbic efficiency and short-cycle life [4–6]. Further, lower-order polysulfides (Li_2S_x, $2 < x \leq 1$) i.e., lithium sulfide Li_2S_2 and/or Li_2S, exhibit poor electronic and ionic conductivity which forms sluggish kinetic process and poor utilization of active material. Additionally, the volume changes during cycling due to different density of sulfur and Li_2S lead to internal strain and unstable interfaces in electrochemistry [7,8].

Over the past decade, researchers have made significant efforts to overcome these hurdles and have come up with various approaches like the use of conductive carbon–sulfur composites to resolve poor conductivity [4], metal oxide additives, and protective interlayers for trapping polysulfide, etc. [9]. To impede the shuttle effect, the diffusion mechanism of polysulfide can be suppressed by physical and chemical trapping. The different carbon materials like carbon nanotubes, carbon nanofibers, carbon nano-spheres, graphitic carbon nano-cages, and different polymers can restrict the polysulfides by physical trapping [10]. The polysulfide suppressing by chemical adsorption is also possible in these carbon materials by the doping of heteroatoms such as nitrogen [11], boron [12], boron-nitrogen [13], nitrogen-boron-oxygen [14], etc. [15]. There are various approaches that serve for chemical and physical suppressing of polysulfides such as core–shell morphology [16], hybrid sponge structure [17], and electrode modification by a thin coating layer over the electrode [18–20]. The modification of electrode and different morphologies improve the electrochemical performance but it affects the active mass loading that leads to a reduction in the energy density of the battery [2]. Therefore, the modification of separator and introducing an interlayer is a better solution to suppress the polysulfides without reducing the active material (Sulfur) of the

* Corresponding author at: Creative & Advanced Research Based On Nanomaterial (CARBON) Laboratory, Department of Chemical Engineering, Indian Institute of Technology, Hyderabad 502285, Kandi, Sangareddy, Telangana, India.
E-mail address: csshama@che.iith.ac.in (C.S. Sharma).
[1] These two authors contributed equally to this work.

https://doi.org/10.1016/j.apsusc.2020.147483
Received 12 July 2020; Received in revised form 4 August 2020; Accepted 6 August 2020
Available online 09 August 2020
0169-4332/

electrode [21]. Separator is an important component of the battery, which provides path to ions and also prevent direct contact between cathode and anode, hence avoid short circuit. However, it is observed that the direct coating of conducting nanomaterials over the separator leads to short circuits [21]. Thus introduction of an interlayer between cathode and separator emerges out to be the best solution for polysulfide trapping, and volume expansion [22–25]. The active site of conductive and porous interlayer helps in the conversion of polysulfides (high order to lower-order polysulfides), and also serves as the upper current collector to improve the electron movement [21]. Further, interlayer acts as buffer additive for sulfur and also facilitates in overcoming volume expansion [6]. Manthiram etal.'s [2] work opened up the broad field of conductive and porous carbon interlayer which included multi-walled CNT, meso-microporous and functionalized carbon for Li-S battery [21]. Many groups explored the different materials for interlayer which include graphene on polypyrrole [26], bacterial cellulose derived nanofibers [27], polypyrrole nanotube mesh [28], acetylene black mesh [29], nitrogen-doped graphene [11], and few more. Oxides are also well known for polysulfide adsorption due to the fact that sulfur has an affinity towards the oxygen present in metal oxides [30]. David Sichen Wu et al. demonstrated a quantitative analysis of various oxides i.e. V_2O_5, MnO_2, V_2O_3, TiS_2, and FeS, signifying their strong interactions with polysulfide [31]. Sarish Rehman et al. explained that Si/SiO_2 can anchor the movable and soluble polysulfides and trap them within its hybrid spheres via chemical binding and reduce the active mass loss [32]. The hybrid spheres of SiO_2 desorb the trapped polysulfides during oxidation, making them accessible as active sulfur cathode material. SiO_2 also facilitates uninterrupted electron supply through a micro-mesoporous carbon shell which further improves the electrochemical stability, resulting in enhanced reversible storage capacity [15]. Xiang et al. demonstrated the suppression of polysulfides by both physical as well as chemical interaction with mesoporous silica structure and reported the electrochemical performance of 574 mAh g^{-1} at 4C by enhancing the Li-ion transport and electrolyte wettability. Aswathy Raghunandanan et al. demonstrated the surface modified graphite paper matrix with high sulfur loading exhibiting good coulombic efficiency and rate capability [33]. There are also other studies, which prove the effective behavior of graphite and silica to trap the polysulfides.

Herein, we present a facile, economic, binder-free, and freestanding hierarchical pencil graphite coated pyrolyzed cellulose paper as an interlayer. The pencil graphite is composed of graphite and clay (mainly SiO_2 [34]) whose ratio varies with the grade of pencil (4B, HB and 5H). We studied the electrochemical performance of Li-S cell with an interlayer (IL) fabricated using different grades of pencil (XX) over the cellulose filter paper (CP) i.e. (Py_XX_CP_IL). The hierarchical structure of interlayer due to graphite and silica particles (from the pencil) over micron sized cellulose fibers provides the active sites to trap polysulfides and at the same time, provides conductivity for effective utilization of active material i.e. sulfur. Furthermore, we have performed the first principle calculation based on density functional theory (DFT) to investigate the interaction between polysulfides and graphite/silica structures (present in interlayer). Li-S battery with Py_HB_CP_IL exhibits an initial capacity of 1352 mAh g^{-1} and 995 mAh g^{-1} at the current density of 100 and 500 mA g^{-1} respectively which is significantly more than Py_4B_CP_IL and Py_5H_CP_IL respectively. The electrochemical impedance spectroscopy (EIS) studies also provide an evident proof that charge transfer resistance is less in the case of Py_HB_CP_IL pencil grade as compared to Py_4B_CP_IL and Py_5H_CP_IL. The prominent reason for the difference in electrochemical performance may be due to the stoichiometric ratio of graphite and silica present in different grades of pencil. Hence, all the further physical and electrochemical characterization have been performed with Py_HB_CP_IL. To study the effect of pencil coating, the electrochemical results of Py_HB_CP_IL are also compared with only pyrolyzed cellulose paper interlayer (Py_CP_IL) and without interlayer.

2. Experimental section

2.1. Electrode preparation, fabrication of pyrolyzed pencil coated interlayers and preparation of polysulfide solution

2.1.1. Electrode preparation

To prepare the cathode, sulfur (Sigma Aldrich), super P carbon black (TIMCAL) and polyvinylidene fluoride (PVDF) (Kynar, Japan) were grinded in 70:20:10 wt ratio for 2 h. N-methyl pyrrolidone (NMP) (Sigma Aldrich) solvent was used to prepare cathode slurry, which was coated uniformly over stainless steel (SS) (MTI Corporation, CA, USA) collector with a thickness of 10 μm. Sulfur electrodes were placed in a vacuum oven at 60 °C for 12 h after evaporation of solvent at room temperature.

2.1.2. Fabrication of pyrolyzed pencil coated interlayers

The commercially available pencil of different grade i.e. 4B, HB, 5H is coated uniformly on one side of the cellulose filter paper of 12.5 cm diameter, 180 μm thickness and pore size 11 μm (Whatman Grade 1, Sigma Aldrich). The cellulose paper and pencil coated cellulose paper are loaded in the high temperature furnace (Nabertherm) and pyrolyzed at a rate of 2 °C min^{-1} at 350 °C for 30 min and 900 °C with a rate of 5 °C min^{-1} for 1 h under an argon (Ar) atmosphere at flow rate

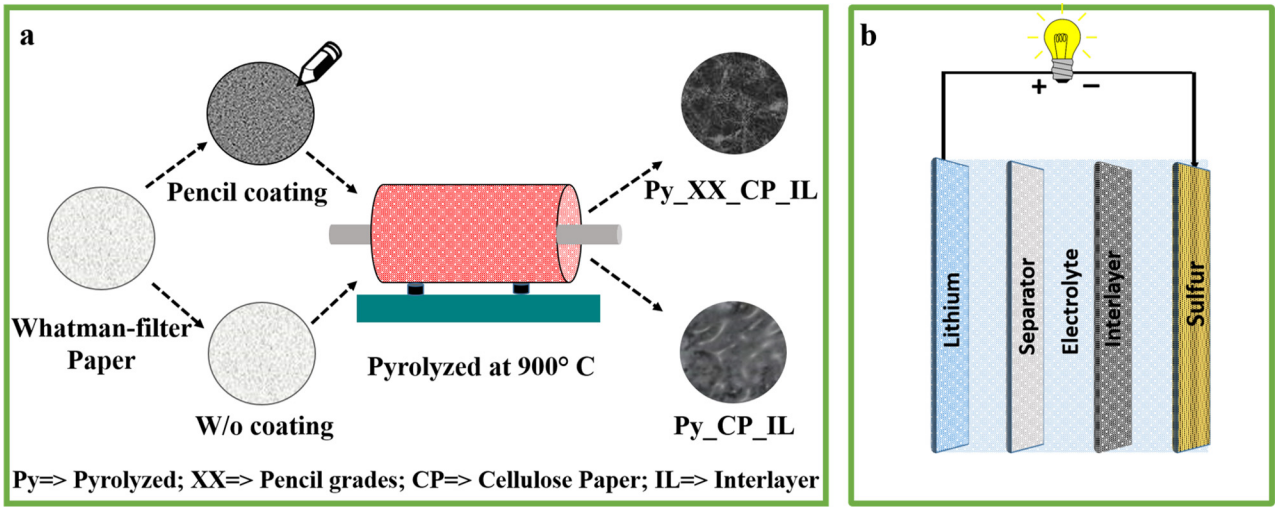

Fig. 1. Schematic for (a) fabrication of interlayer and, (b) Li-S cell assembly with interlayer.

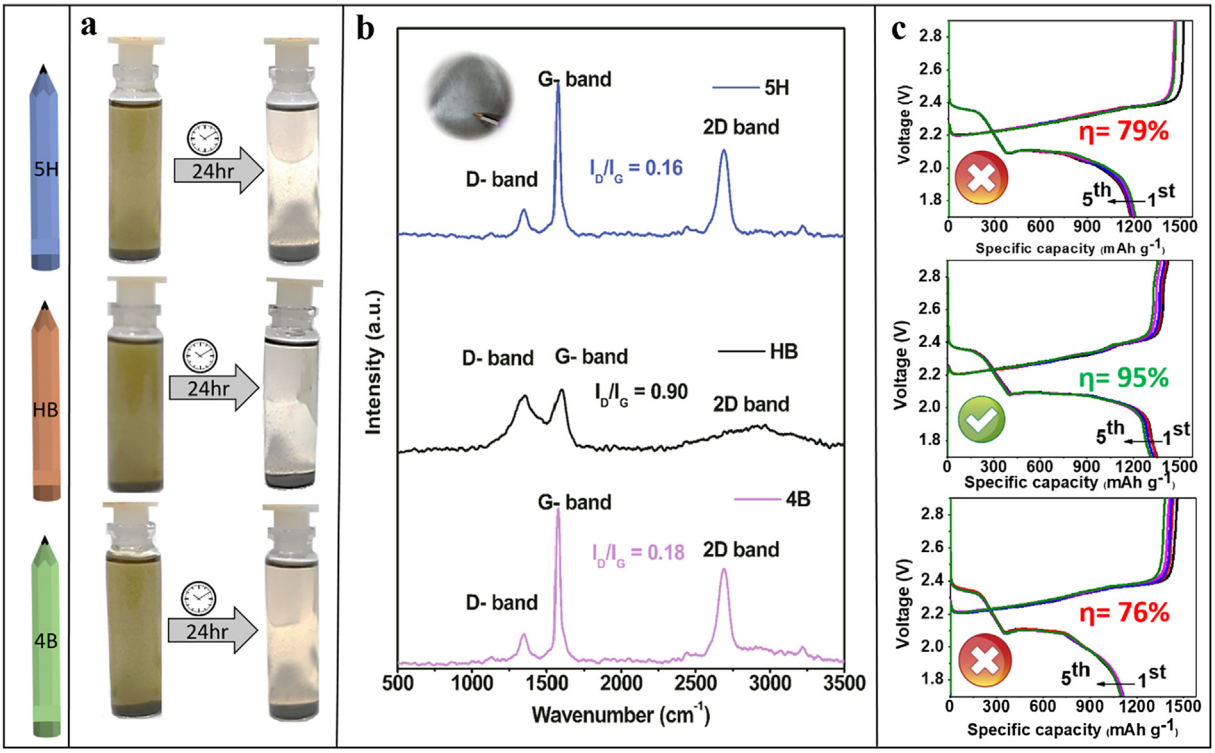

Fig. 2. (a) The adsorption studies using different pencil grade powder (5H, HB, and 4B), (b) Raman analysis of the fabricated interlayers using a different grade of pencil, and (c) Comparative galvanic charge–discharge curves at 0.1 mA g^{-1} current density for different grade of pencil.

of 0.5 cc. The pyrolyzed sheet was cut into a 19 mm diameter using disk cutter to use as an interlayer and placed in between sulfur cathode and separator. The weight of interlayer was maintained the same (0.16 mg cm^{-2}) for all the pencil coated interlayer samples (Fig. 1a).

2.1.3. Preparation of polysulfide solution for adsorption studies

Sulfur and Li_2S (Sigma-Aldrich) were added to Dioxolane (DOL) and Dimethoxyethane (DME) (Sigma Aldrich) with (1:1 in volume) to form a molar ratio of 5:1. The solution was stirred for 12 h at 80 °C under Ar-atmosphere [27].

2.2. Structural and chemical characterization

Structural characterization of the material was conducted by field emission scanning electron microscopy (FESEM) (JEOL-JEM-2011(200KV)) and transmission electron microscopy (TEM) (JEOL-JSM-700F). Raman spectra (WITec Raman spectroscopy) was obtained by using green laser excitation (λ = 532 nm with excitation energy of 2.33 eV). The specific surface area and pore size distribution of interlayers was analyzed using N_2 adsorption isotherms (Autosorb iQ, Quantachrome, USA). The absorbance of polysulfide was measured using UV–vis spectrometer (UV 3092; LabIndia Analytical Pvt. Ltd.). X-ray diffraction (PANalyticaX'pert pro-X-ray diffractometer) of the sample was recorded with Cu-Kα radiation (λ = 0.154 nm) source.

2.3. Li-S cell assembly and electrochemical testing

Sulfur cathode electrode and freestanding graphite coated pyrolyzed cellulose filter paper interlayers were dried in a vacuum oven for an hour at 60 °C. The CR2032 coin-type cell was assembled with sulfur cathode, interlayer (the coated side facing towards sulfur cathode), polypropylene separator (Celgard 2500), lithium anode (Sigma Aldrich) and stainless steel spacer with spring in an argon-filled glove box (Mbraun, O_2 < 0.1 ppm, H_2O < 0.1 ppm) (Fig. 1b). Electrolyte (10 µl) was drop cast over polypropylene separator, containing 1 M Bis (trifluoromethylsulfonyl)amine lithium salt (LITFSI) in DOL: DME (1:1 vol ratio) and 0.1 M $LiNO_3$ as electrolyte additive. The weight of sulfur cathode for Py_4B_CP_IL, Py_HB_CP_IL, and Py_5H_CP_IL cell was 1.86, 1.85 and 1.90 mg respectively. Cyclic voltammetry (CV) was conducted at scan rate of 0.1 mV s^{-1} in voltage range of 1.7 to 3.0 V (vs. Li/Li^+). The EIS was performed at frequency range of 0.1 Hz-0.1 M Hz with disturbance amplitude set at 10 mV. All the electrochemical testing was carried out using Biologic VSP 300 electrochemical workstation at ambient room temperature.

2.4. Calculation method

The structure optimization and thermodynamic energy calculations were performed using Gaussian 09 software package with the B3LYP/STO-3G level of theory, reported in the previous work [35–41]. The total binding energy (ΔE_T) between polysulfides and graphite/silica structures was computed using the following equation.

$$\Delta E_T = E_{PS+Gr/SiO_2} - \left(E_{Gr/SiO_2} + E_{PS}\right)$$

where $E_{PS+Gr/SiO2}$, E_{PS}, and $E_{Gr/SiO2}$ are the total ground state energies of polysulfide adsorbed on graphite/silica structure, polysulfide structure, and bare graphite/silica structures, respectively.

3. Result and discussion

As discussed in previous section and shown in schematic Fig. 1(b), the fabricated hierarchical nanostructured interlayer embedded with graphite and silica particles was placed in between separator and sulfur cathode. The graphite coated side of the interlayer was faced towards the cathode. We used three grades of pencil i.e. 4B, HB, and 5H to understand the effect of graphite and clay (silica) content present in pencil-coated interlayer.

The variation of graphite and clay with the pencil grade is provided in Table S1. 4B pencil contains a higher percentage (79%) of graphite compared to HB (68%) and 5H (52%) [42]. However, silica content in

4B pencil (15%) is lower than HB (26%) and 5H (42%) [43]. Polysulfide adsorption test was performed with fine powder of different pencil grades (1 mg) dispersed in lithium polysulfide (Li_2S_6) solution as depicted in Fig. 2(a). A clear solution in the vials after 24 h, evidently shows that all pencil grades tend to absorb the polysulfides. However, it was observed that the adsorption was faster in the case of 5H due to high content of clay (silica), as compared to 4B and HB pencil. Raman spectra analysis confirmed the graphite content present on the pencil coated side of (Fig. 2(b)) cellulose fibers. It shows three distinctive peaks at ~1350, ~1580, and ~2752 cm^{-1} corresponding to D-band, G-band, and 2D-band, respectively. D-band stands for A_1g stretching vibrations which relates to the disorder and structural defects present in carbon [44]. G-band indicates the vibration of sp^2 bonded carbon atom [45]. The typical 2D peak confirms the few-layered structure of graphene [46]. The calculated I_D/I_G ratio of 4B, HB, and 5H pencil on cellulose paper is 0.16, 0.90, and 0.18, respectively. The I_D/I_G ratio of HB interlayer represents higher degree of disorder in carbon atom compared to 4B and 5H [47]. The galvanic charge–discharge test was performed at 100 mA g^{-1} to quickly check the electrochemical performance of cells fabricated using different interlayers i.e. 4B, HB, 5H.

The graph (Fig. 2(c)) shows typical two plateau behavior of sulfur cathode which correspond to the formation of higher-order polysulfide i.e. long-chain formation (Li_2S_X ($8 \geq X \geq 4$)) at 2.3 V and lower order polysulfide i.e. short-chain formation (Li_2S_2 and Li_2S) at 2.1 V. As fabricated Li-S cells exhibits specific capacity of 1101, 1352, and 1173 mAh g^{-1} at 100 mA g^{-1} current density with coulombic efficiency of 76%, 95%, and 79% for Py_4B_CP_IL, Py_HB_CP_IL, and Py_5H_CP_IL, respectively. Also, 780, 980 and 838 mAh g^{-1} at 500 mA g^{-1} current density respectively as shown in Fig. S1. Thus, Py_HB_CP_IL prevents shuttling of polysulfide and shows better performance in terms of specific capacity with coulombic efficiency of 95%. This can also be related to the lower charge transfer (R_{CT}) and solution resistance (R_S) of Py_HB_CP_IL (10.69 and 15.39 Ω) compared to Py_4B_CP_IL (13.35 and 17.27 Ω) and Py_5H_CP_IL (15.91 and 22.15 Ω) as shown in Table S1 and Fig. S2. The enhanced performance of Py_HB_CP_IL interlayer motivates us to investigate it further using various micro-imaging, structural and electrochemical characterizations. Further, we compare the electrochemical performance of Py_HB_CP_IL with pyrolyzed cellulose paper (Py_CP_IL) interlayer and without interlayer (W/o_IL) for Li-S cell.

The first principle calculations based on DFT are used to investigate the interaction between polysulfides and graphite/silica structures (present in interlayer). To represent the graphite system, a carbon sheet composed of 7 benzene rings and silica (Si_8O_{10}) was used in the present study. A hydrogen atom terminated the edge atom of silica and graphite structure. Fig. 3a, b shows the optimized structure of graphite, silica and graphite/silica interaction with polysulfide (Li_2S_4). Initially, each structure was individually optimized and then their interaction system (graphite/silica interaction with polysulfide (Li_2S_8, Li_2S_6, Li_2S_4)) was fully optimized at the B3LYP/STO-3G level of theory. Fig. S3 shows the final optimized structure of graphite/silica interaction with polysulfide (Li_2S_6 and Li_2S_8).

The calculated interaction energy between various polysulfides (Li_2S_8, Li_2S_6, and Li_2S_4) with graphite and silica is depicted in Fig. 3c. Here, greater the (negative) interaction energy ΔE_T (kJ/mol) means stronger interaction of polysulfide with graphite/silica structures and thus is thermodynamically preferred.

The calculated binding energy of polysulfides with silica structure is −544.2, −375.9, and −470.7 KJ/mol for Li_2S_8, Li_2S_6, and Li_2S_4, respectively. Whereas, the binding energy of graphite with polysulfides is −26.25, −52.5 and −78.76 KJ/mol for Li_2S_8, Li_2S_6, and Li_2S_4, respectively. This calculated result demonstrated that the adsorption properties of silica material towards soluble polysulfide is thermodynamically favorable and stable compared to the carbon-based graphite material. This could be due to the polar nature of silica material over the non-polar nature of graphite [32,48]. This polar nature of silica will help the chemical anchoring of lithium polysulfide and prevent its dissolution [49]. However, the electrical conductivity of graphite is in the order of 10–10^4 S cm^{-1} [50] and for silica is 5 × 10^{-12} S cm^{-1} [51]. Thus, the graphite provides much necessary conductive support to the interlayer (required for polysulfide reduction) whereas silica provide polysulfide adsorption. Therefore, this pencil-based interlayer is designed as a preferred combination of silica and graphite, which will provide efficient adsorption sites (from silica) for polysulfide, and provides the conductivity to trapped polysulfides (from graphite) to significantly facilitate the oxidation of Li_2S back to sulfur.

3.1. Physiochemical characterization

As investigated further, the hierarchical morphology of Py_HB_CP_IL is confirmed with SEM and TEM micrograph as shown in Fig. 4. The side of interlayer without coating has cellulose derived hollow micro carbon fibers shown in Fig. 4(a). Uniform coating of graphite and SiO_2 particles over the carbon fibers can be noticed on the other side (with pencil coating) of interlayer in Fig. 4(b). The elemental mapping confirmed homogeneous distribution of carbon, oxygen, and silicon throughout the interlayer (Fig. 4(c)). Carbon in the form of graphite provides conductivity to reduce higher-order polysulfides to lower-order polysulfide [43]. The enhanced surface area can also serve the volume expansion during the discharging in the conversion of S_8 to Li_2S [7].

Crumpled graphite sheets with silica nanoparticles can be observed in TEM micrograph as shown in Fig. 4(d) [52]. This structure includes graphite sheets, and silica nanoparticles [34,53] from pencil and carbon microfiber (Fig. 4(e)) from cellulose filter paper. The hierarchical structure of carbon microfiber with graphite sheets and silica nanoparticles on its surface can be further confirmed from Fig. 4(e, f). The turbostratic carbon nanostructure derived from organic carbon (i.e. cellulose fibers) can be observed in Fig. 4(f), with a lattice spacing of 0.33 nm [54]. This nanostructure will help to provide electrical conductivity via nanoscale aromatic linkage [55].

X-ray diffraction pattern of the Py_HB_CP_IL interlayer with a prominent graphitic peak at 26.7° and the remaining diffraction peaks of silica (JCPDS file: 046–1045) can be observed from Fig. 5(a) [56]. FTIR analysis of Py_HB_CP_IL confirmed the presence of O—H, C—H, C—O, C═O, C—H stretching at 3427 2962, 1260, 1022 and 787 cm^{-1}, respectively, as shown in Fig. 5(b) [53].

These functional groups provide chemical affinity towards polysulfides, hence help in polysulfide trapping [57]. The peaks at 1404, 1092, and 687 cm^{-1} are attributed to stretching vibrating of Si—O, Si—O—Si, and Si—O groups of siloxane respectively which confirm the presence of silica [53,58–60]. A distinct hysteresis loop can be identified (i.e., Type-IV) from N_2 adsorption–desorption isotherm which indicates the mesoporous structure present in interlayer as shown in Fig. 5(c). The Py_HB_CP_IL has BET surface area of 440.3 m^2 g^{-1} and average pore size of 3.3 nm (Fig. 5(d)). The micro and mesopores present in the interlayer are considerably effective to trap polysulfides because the bond length of Li-S, S-S, and long-chain polysulfide is ≈2 nm [21]. The high surface area not only provides ample porous structure to accommodate more sulfur but also provides the copious adsorption and catalytic sites for the polysulfides, thus considerably improving both the specific capacity and cycling performance of Li-S batteries.

3.2. Electrochemical performance

The Li-S cell was fabricated to compare the electrochemical performance of Py_HB_CP_IL with Py_CP_IL and without any interlayer (W/o_IL). Fig. 6(a) shows CV for all three cases; the traditional cathodic peaks were observed at 2.31, 2.33 and 2.3 V, respectively which correspond to the transition of S_8 to higher ordered polysulfide Li_2S_x ($4 < x < 8$) such as Li_2S_4, Li_2S_6, Li_2S_8 [28]. Further, cathodic peaks at

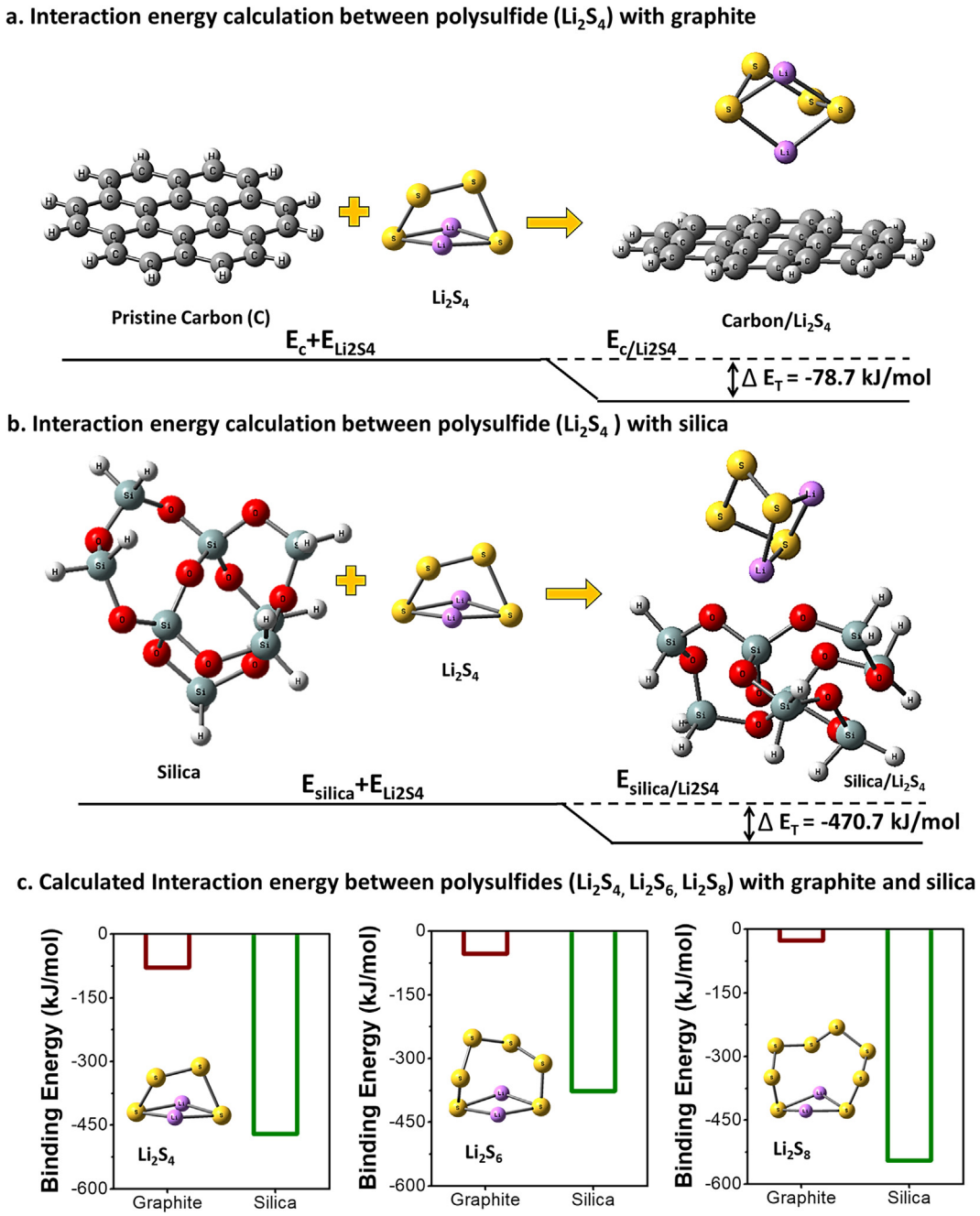

Fig. 3. DFT calculations: (a) a schematic representation of interaction energy calculation between polysulfide (Li_2S_4) with graphite, (b) a schematic representation of interaction energy calculation between polysulfide (Li_2S_4) with silica, and (c) calculated interaction energy between polysulfides (Li_2S_4, Li_2S_6, Li_2S_8) with graphite and silica structure.

2.01, 2.03 and 1.9 V respectively correspond to reduction of higher ordered polysulfide to the lower-order polysulfides Li_2S_x ($4 < x < 1$) such as Li_2S_2, Li_2S [28]. The consequent anodic peak shows the broad two-step peak associated with the formation of intermediate products during the reverse conversion from Li_2S_x to S_8 [2]. The rate capability is investigated at different densities of 0.1, 0.5, 1 and 2 A g^{-1}, as shown in Fig. 6(b). In the case of the W/o_IL, the cell exhibited a very low capacity of 388, 203, and 127 mAh g^{-1} at 0.1, 0.5, 1 A g^{-1}, respectively which maybe because of less utilization of active material. In the case of Py_CP_IL, the cell showed discharge capacity of 890, 562, 430, and 196 mAh g^{-1} at 0.1, 0.5, 1 and 2 A g^{-1}, respectively. However, initial discharge capacities of Py_HB_CP_IL are much improved and are 1346, 969, 862, and 710 mAh g^{-1} at 0.1, 0.5, 1 and 2 A g^{-1}, respectively with the same discharge capacity during back cycling. The cyclic stability of the cells was carried out at a current density of 1A g^{-1} for 350 cycles as shown in Fig. 6(c). Py_HB_CP_IL cell showed a capacity of 725 mAh g^{-1} with a capacity retention of 90% after 350 cycles. Whereas Py_CP_IL cell delivered a capacity of 199 mAh g^{-1} over 140 cycles with columbic efficiency of 84%. This clearly shows that the Py_CP_IL has not been effective due to less active sites to trap polysulfides as compare to Py_HB_CP_IL. The EIS was performed before and after cycling as shown in Fig. 6(d). The high-frequency region indicates electrolyte resistance (R_s) of the cell. The semicircles at the high-frequency region represent the charge transfer resistance (R_{ct}) [61]. The Py_HB_CP_IL offers the low charge transfer resistance compared to the Py_CP_IL interlayer cell as shown in Table S2. This could be due to the graphite wrapped around the carbon cellulose fibers, which improved the conductivity of the structure. Although, silica particles are insulating in nature, but an

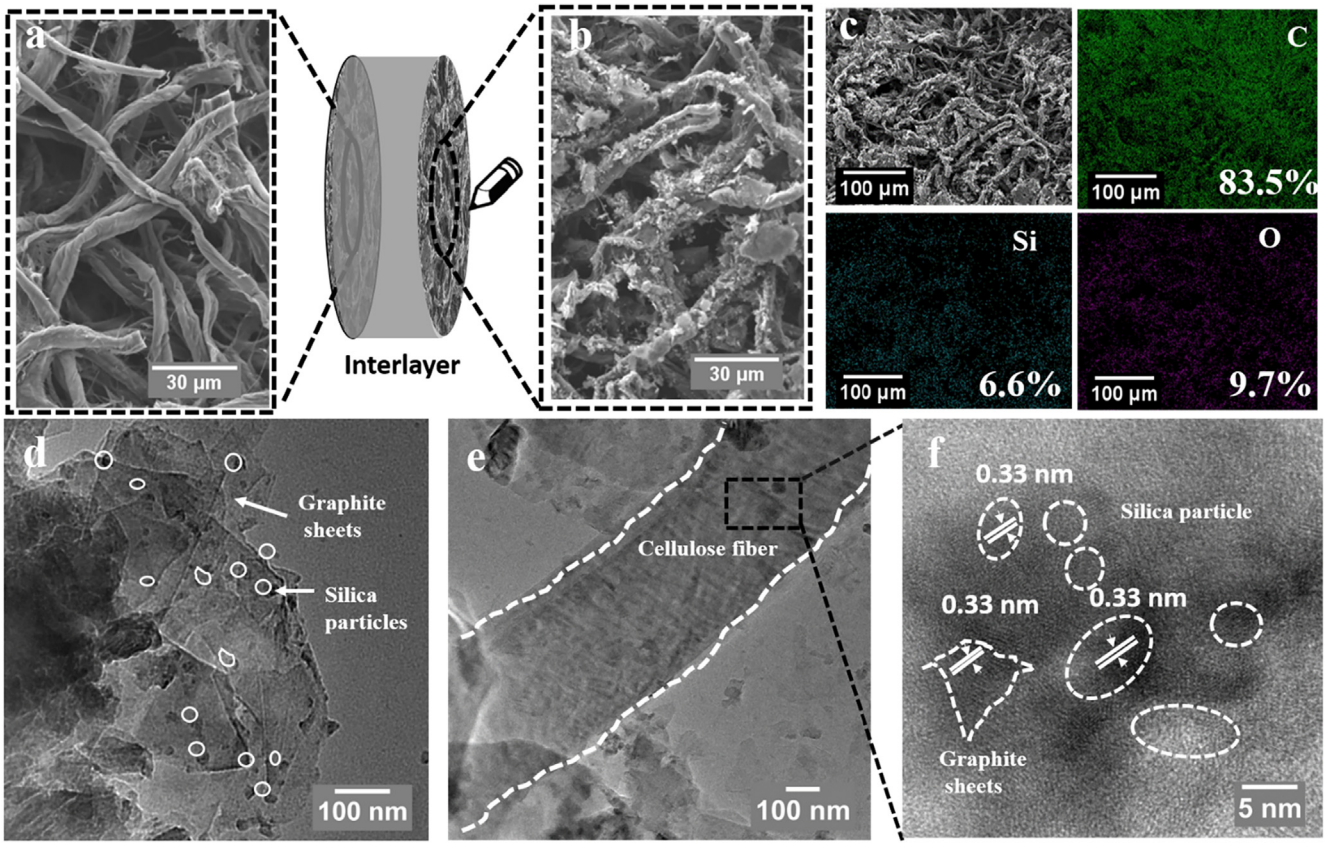

Fig. 4. Schematic of interlayer with FESEM images (a) without coating side, (b) HB pencil coating side, (c) EDX of HB pencil coating side with the elemental mapping of carbon (C), Silicon (Si) and oxygen (O), TEM image of (d) folded graphite sheets, (e) cellulose carbon fiber with HB pencil coating, (f) zoomed image of fiber with a lattice spacing of graphite sheets and silica particles.

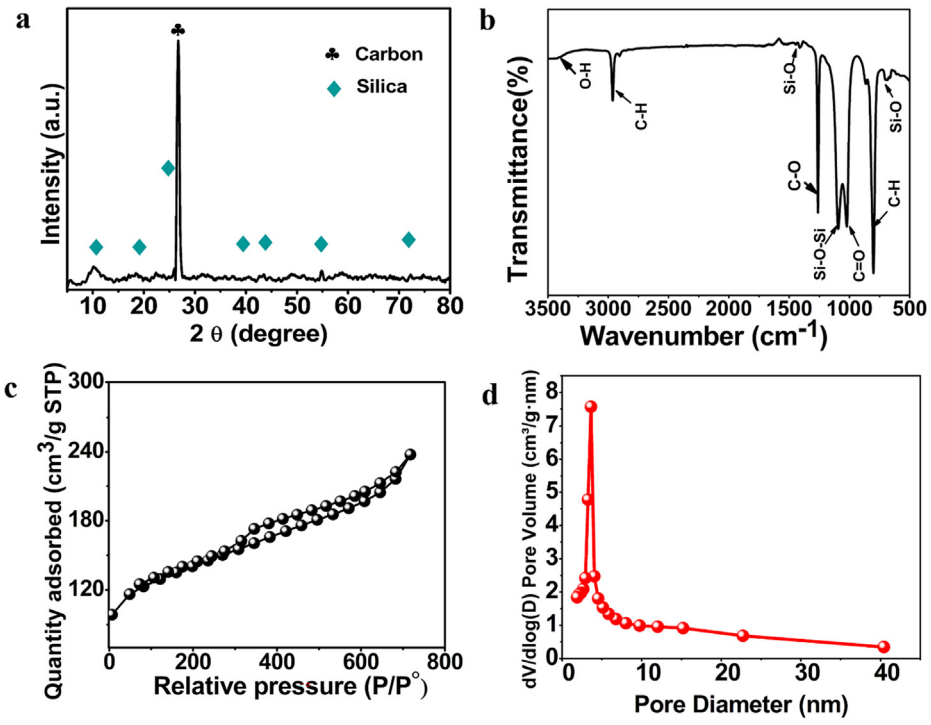

Fig. 5. (a) XRD pattern (b) FTIR spectra, (c) BET) surface area analysis and (d) Pore size distribution for Py_HB_CP_IL.

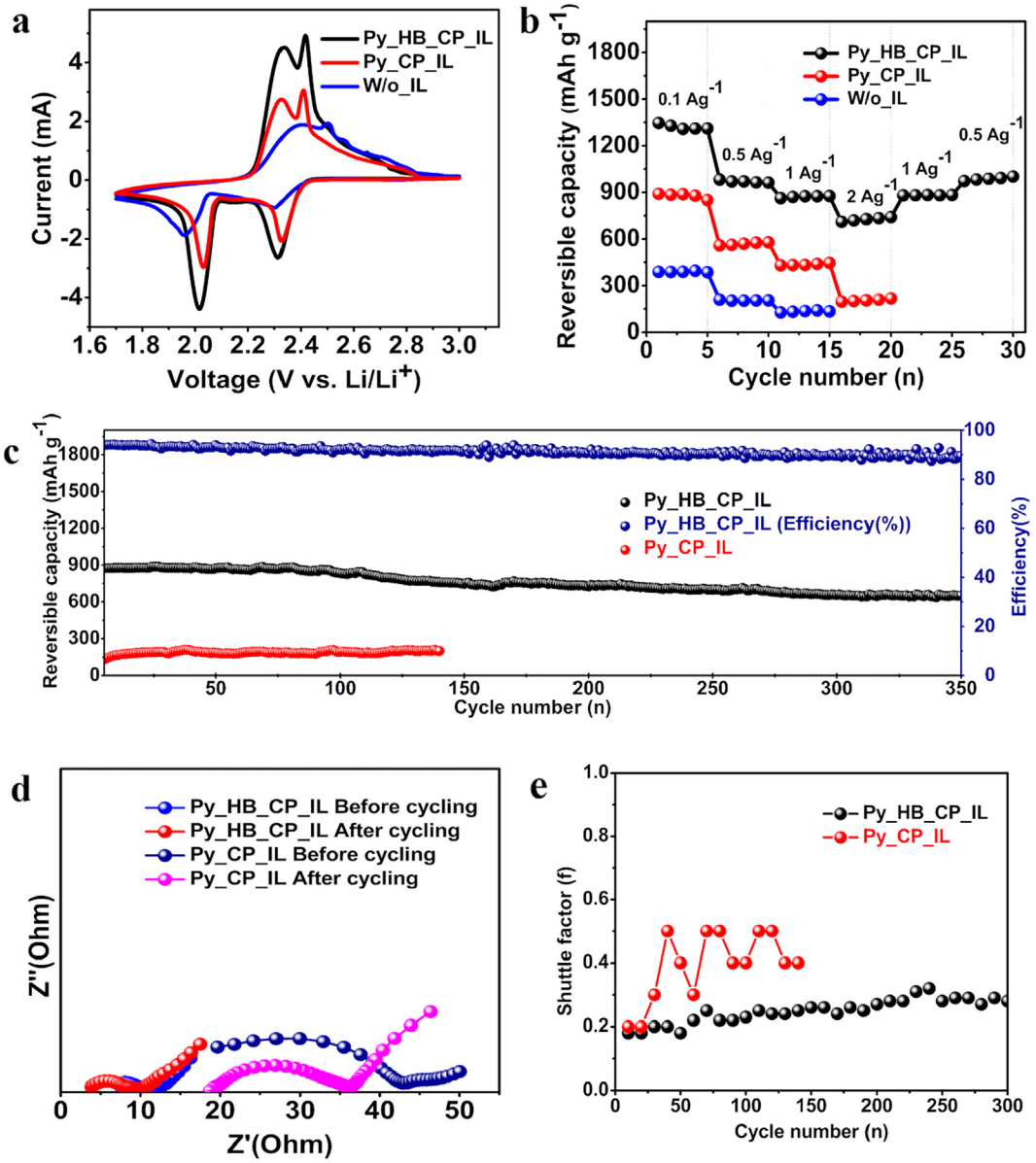

Fig. 6. (a) CV analysis, (b) rate capability for Py_HB_CP_IL, Py_CP_IL, and W/o_IL at different current density, (c) cyclic stability at 1 Ag^{-1} current density, (d) Before and after cylicing EIS analysis, and (e) Shuttling factor of Py_HB_CP_IL and Py_CP_IL.

optimum ratio of graphite and silica nanoparticles in HB pencil overcame this issue. Thus, the micro range carbon fibers with silica nano range particle and graphite as an additive interact favorably to reduce the overall charge transfer and diffusion resistance that further improve the electrochemical performance of the cell. Thus, Py_HB_CP_IL cell showed enhanced electrochemical performance by overcoming the shuttling of polysulfides from cathode to anode.

Furthermore to quantify this shuttling effect, we have calculated the shuttle factor as proposed by Mikhaylik et al. [62] and is shown in Fig. 6(e). Here, higher value of the shuttle factor indicates more polysulfide shuttling. The shuttle factor of Py_HB_CP_IL cell (Fig. 5(e)) for 350 cycles at the current density of 1A g^{-1} is found to be in between 0.2 and 0.25 however in case of PY_CP_IL, it is calculated to be in the range of 0.2 to 0.5. The low shuttle factor in the case of Py_HB_CP_IL clearly indicates that the HB pencil coated interlayer is serving its purpose because of the silica and graphite present in it.

We have then performed FESEM and EDX post cycling (after 350 cycles) to confirm the trapping of polysulfides in the interlayer as shown in Fig. 7. FESEM micrograph clearly shows that the interlayer's fibers were intact even after long cycling (Fig. 7(a, b)). The EDX analysis showed that the cathode facing side of interlayer has 11.2% of the elemental sulfur whereas on the opposite side, it's only 1.2%. This confirms that the interlayer efficiently trapped the polysulfides by not allowing them to pass through it. To further prove the effective role of Py_HB_CP_IL in prohibiting the diffusion of polysulfides, we have performed a polysulfide permeability test using a H-cell setup. The test was performed with Py_HB_CP_IL and W/o_IL as shown in Fig. 8. Left side of the H-cell setup was filled with a controlled polysulfide solution and the right side has only DOL/DME electrolyte solution. The change in color (right side) started for W/o IL after 6 hrs.

This indicates that polysulfides are moving from the left-side reservoir to the right side. However, in the case of Py_HB_CP_IL, there was no change in color observed even after 24 h. This visual evidence also suggests that the Py_HB_CP_IL has a strong ability to trap the polysulfide due to the presence of hierarchical structure with carbon cellulose fiber, silica nanoparticles, and pencil graphite. Moreover, to confirm and quantify this result, we have performed UV–vis spectroscopy analysis for the samples collected from the right side of the H-cell at 0 h and

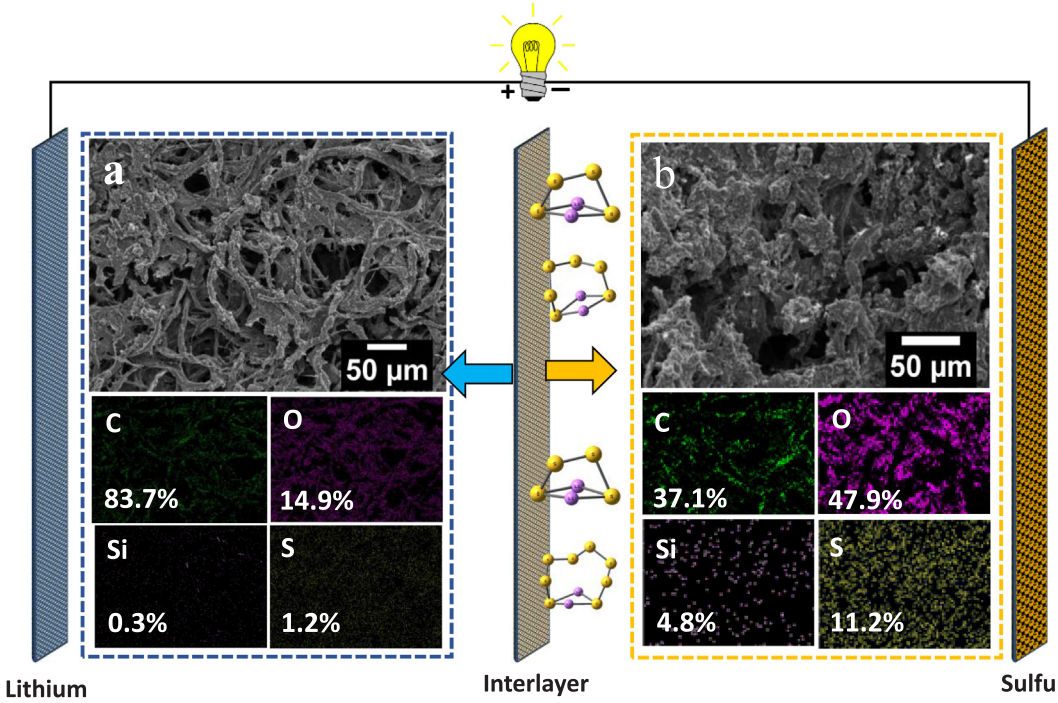

Fig. 7. Post cycling analysis: FESEM images and EDX elemental mapping of interlayer after 350 cycles (a) separator facing side of the interlayer, (b) cathode facing side of the interlayer.

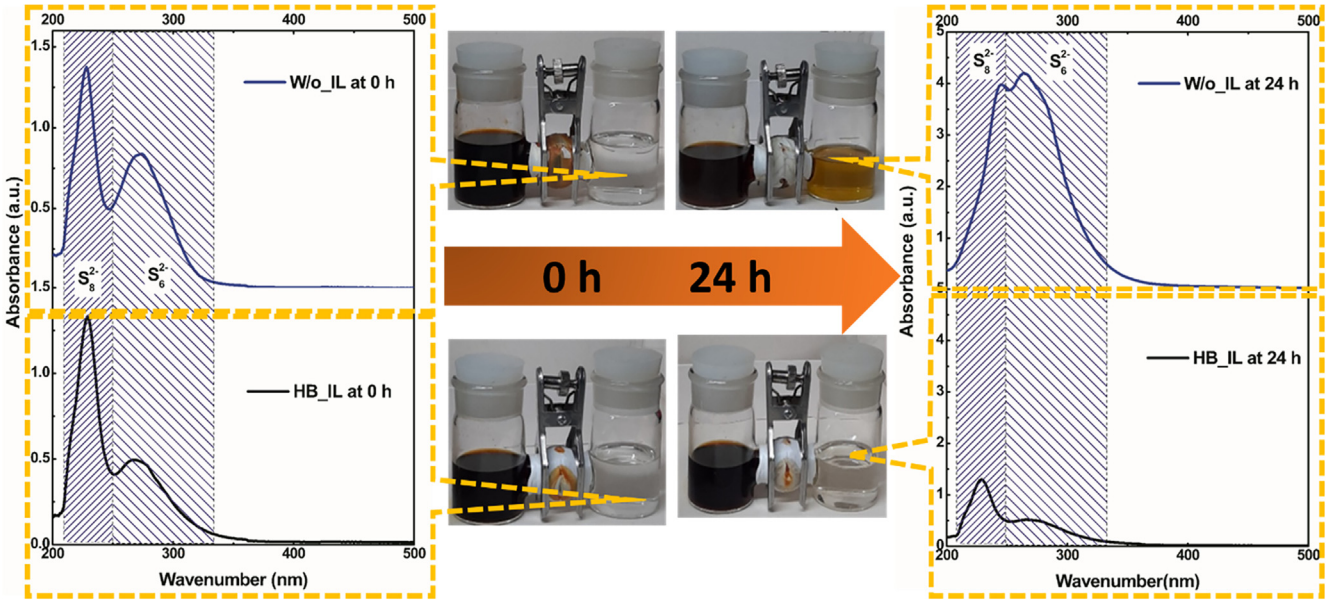

Fig. 8. The polysulfide permeability test using the H-cell setup and UV–vis spectra of the collected samples at 0 and 24 h.

24 h. The collected solution from H-cell with Py_HB_CP_IL after 24 h shows significantly low adsorption compare to the W/o_IL. This again confirms that Py_HB_CP_IL efficiently trapped the polysulfide. The different interlayer strategies for Li-S batteries as reported in literature are summarized in Table S3 [28,57,63–69], which shows the effectiveness of the current work as compared to the available literature to improve the overall electrochemical performance of Li-S battery.

4. Conclusion

We have designed a novel, low-cost, and scalable pyrolyzed pencil graphite coated cellulose paper as an interlayer for high-performance lithium-sulfur battery. We studied and compared the effect of three different grades of pencil (4B, HB, and 5H) over cellulose paper for Li-S performance. Interlayer with HB pencil graphite outperformed 4B and 5H based interlayers because of the optimum stoichiometric ratio of graphite and clay (silica) content. Further, we have compared the electrochemical performance of Py_HB_CP_IL with Py_CP_IL and W/o_IL. Here, Py_HB_CP_IL delivered a three-fold increase and Py_CP_IL delivered a two-fold increase in capacity as compared to W/o_IL for Li-S cell. This improvement is observed due to the synergistic effect of graphite and silica particles over cellulose carbon fibers. The silica particles and oxygen present in cellulose carbon fiber traps the polysulfide due to dipole–dipole electrostatic interaction. Further graphite over carbonized cellulose fibers provides a conducting path for ions and reduce the contact resistance between cathode active material and

separator. This binder-free, highly efficient, and frugal interlayer strategy is successfully proven in detail as a better alternative to significantly improve the electrochemical performance of Li-S battery and to realize the commercial feasibility.

CRediT authorship contribution statement

Poonam Rani: Investigation, Methodology, Data curation, Formal analysis, Writing - original draft. **Krishna S. Kumar:** Investigation, Methodology, Data curation, Formal analysis, Writing - original draft. **Anil D. Pathak:** Investigation, Formal analysis, Writing - review & editing. **Chandra.S. Sharma:** Conceptualization, Supervision, Resources, Writing - review & editing, Funding acquisition.

Declaration of Competing Interest

The authors declare that they have no known competing financial interests or personal relationships that could have appeared to influence the work reported in this paper.

Acknowledgment

We would like to acknowledge the Ministry of Human Resources & Development and Department of Heavy Industries, Govt. of India for the financial support under the IMPRINT I scheme (project no. 7035) to carry out this work. The authors also acknowledge to Dr. Akhilesh Kumar Singh at IIT Bhubaneswar for providing computational resources for DFT calculations. Poonam Rani acknowledges the technical discussions with Illa Mani Pujitha related to this work.

Appendix A. Supplementary material

Supplementary data to this article can be found online at https://doi.org/10.1016/j.apsusc.2020.147483.

References

[1] Placke, Tobias1. Placke, T., Kloepsch, R., Dühnen, S. & Winter, M. Lithium ion, lithium metal, R. Kloepsch, S. Dühnen, M. Winter, Lithium ion, lithium metal, and alternative rechargeable battery technologies: the odyssey for high energy density, (2017). Doi: 10.1007/s10008-017-3610-7.

[2] A. Manthiram, Y. Fu, S. Chung, C. Zu, Y. Su, Rechargeable lithium − sulfur batteries, (2014).

[3] R. Chen, R. Luo, Y. Huang, F. Wu, L. Li, Advanced high energy density secondary batteries with multi-electron reaction materials, (2016). Doi: 10.1002/advs.201600051.

[4] Y. Yin, S. Xin, Y. Guo, L. Wan, Lithium – sulfur batteries : electrochemistry, materials, and prospects angewandte, (2013) 13186–13200. Doi: 10.1002/anie.201304762.

[5] Z. Li, Y. Huang, L. Yuan, Z. Hao, Y. Huang, Status and prospects in sulfur-carbon composites as cathode materials for rechargeable lithium-sulfur batteries, Carbon 92 (2015) 41–63, https://doi.org/10.1016/j.carbon.2015.03.008.

[6] Y. Zhang, Y. Peng, Y. Wang, J. Li, H. Li, J. Zeng, J. Wang, J. Hwang, J. Zhao, High sulfur-containing carbon polysulfide polymer as a novel cathode material for lithium-sulfur battery, (2017) 1–9. Doi: 10.1038/s41598-017-11922-6.

[7] Z. Liu, P.B. Balbuena, P.P. Mukherjee, Revealing charge transport mechanisms in Li2S2 for Li-sulfur batteries, J. Phys. Chem. Lett. 8 (2017) 1324–1330, https://doi.org/10.1021/acs.jpclett.6b03063.

[8] X. Yao, N. Huang, F. Han, Q. Zhang, H. Wan, J.P. Mwizerwa, C. Wang, X. Xu, High-performance all-solid-state lithium-sulfur batteries enabled by amorphous sulfur-coated reduced graphene oxide cathodes, Adv. Energy Mater. 7 (17) (2017) 1602923, https://doi.org/10.1002/aenm.201602923.

[9] R. Ponraj, A.G. Kannan, J.H. Ahn, D. Kim, Improvement of cycling performance of lithium-sulfur batteries by using magnesium oxide as a functional additive for trapping lithium polysulfide improvement of cycling performance of lithium-sulfur batteries by using magnesium oxide as a functional addit, (2016). Doi: 10.1021/acsami.5b11327.

[10] [10] Z. Zeng, X. Liu, Sulfur immobilization by “chemical anchor” to suppress the diffusion of polysulfides in lithium – sulfur batteries, 1701274 (2017) 1–40. Doi: 10.1002/admi.201701274.

[11] H. Wu, L. Xia, J. Ren, Q. Zheng, F. Xie, W. Jie, C. Xu, D. Lin, A multidimensional and nitrogen-doped graphene/hierarchical porous carbon as a sulfur scaffold for high performance lithium sulfur batteries, Electrochim. Acta (2018), https://doi.org/10.1016/j.electacta.2018.05.032.

[12] W. Ai, J. Li, Z. Du, C. Zou, H. Du, X. Xu, Y. Chen, H. Zhang, J. Zhao, C. Li, W. Huang, T. Yu, Dual confinement of polysulfides in boron-doped porous carbon sphere/graphene hybrid for advanced Li-S batteries, Nano Res. 11 (2018) 4562–4573, https://doi.org/10.1007/s12274-018-2036-6.

[13] J. Zhu, R. Pitcheri, T. Kang, C. Jiao, Y. Guo, J. Li, Y. Qiu, A polysulfide-trapping interlayer constructed by boron and nitrogen co-doped carbon nanofibers for long-life lithium sulfur batteries, J. Electroanal. Chem. 833 (2019) 151–159, https://doi.org/10.1016/j.jelechem.2018.11.010.

[14] P. Han, A. Manthiram, Boron- and nitrogen-doped reduced graphene oxide coated separators for high-performance Li-S batteries, J. Power Sources 369 (2017) 87–94, https://doi.org/10.1016/j.jpowsour.2017.10.005.

[15] R. Ionescu, S. Ozkan, M. Ozkan, lithium – sulfur batteries, (2015). Doi: 10.1039/c4nr07663j.

[16] J. Wu, N. You, X. Li, H. Zeng, S. Li, Z. Xue, Y. Ye, X. Xie, SiO2@MoS2 core-shell nanocomposite layers with high lithium ion diffusion as a triple polysulfide shield for high performance lithium-sulfur batteries, J. Mater. Chem. A 7 (2019) 7644–7653, https://doi.org/10.1039/c9ta00982e.

[17] X. An, H. Fan, Hybrid design and energy absorption of luffa-sponge-like hierarchical cellular structures, Mater. Des. 106 (2016) 247–257, https://doi.org/10.1016/j.matdes.2016.05.110.

[18] S. Agnoli, M. Favaro, Doping graphene with boron : a review of synthesis, J. Mater. Chem. A: Mater. Energy Sustain. 00 (2016) 1–24, https://doi.org/10.1039/C5TA10599D.

[19] V. Bharti, A. Gangadharan, T.N. Rao, C.S. Sharma, Carbon soot over layered sulfur impregnated coconut husk derived carbon: An efficient polysulfide suppressor for lithium sulfur battery, Mater. Today Commun. 22 (2020) 100717, https://doi.org/10.1016/j.mtcomm.2019.100717.

[20] F. Chen, L. Ma, J. Ren, X. Luo, B. Liu, X. Zhou, Sandwich-type nitrogen and sulfur codoped graphene-backboned porous carbon coated separator for high performance lithium-sulfur batteries, (2018) 1–17. Doi: 10.3390/nano8040191.

[21] Y.C. Jeong, J.H. Kim, S. Nam, C.R. Park, S.J. Yang, Rational design of nanostructured functional interlayer/separator for advanced Li–S batteries, 1707411 (2018) 1–32. Doi: 10.1002/adfm.201707411.

[22] L. Wang, Y.B. He, L. Shen, D. Lei, J. Ma, H. Ye, K. Shi, B. Li, F. Kang, Ultra-small self-discharge and stable lithium-sulfur batteries achieved by synergetic effects of multicomponent sandwich-type composite interlayer, Nano Energy 50 (2018) 367–375, https://doi.org/10.1016/j.nanoen.2018.05.043.

[23] H. Peng, J. Huang, X. Cheng, Q. Zhang, Review on high-loading and high-energy lithium – sulfur batteries, 1700260 (2017) 1–54. Doi: 10.1002/aenm.201700260.

[24] J. Liao, Nontrivial effects of “trivial” parameters on the performance of lithium – sulfur batteries, (2018). Doi: 10.3390/batteries4020022.

[25] K. Zhu, Z. Chi, F. Ke, Y. Yang, A. Wang, L. Miao, i v o r l a n o i v o l, (2019). Doi: 10.3389/fenrg.2019.00123.

[26] [26] Y. Fu, Y. Su, A. Manthiram, Sulfur-polypyrrole composite cathodes for lithium-sulfur batteries, 159 (2012) 1420–1424. Doi: 10.1149/2.027209jes.

[27] S. Li, J. Warzywoda, S. Wang, G. Ren, Z. Fan, Bacterial cellulose derived carbon nano fi ber aerogel with lithium polysul fi de catholyte for lithium e sulfur batteries, Carbon 124 (2017) 212–218, https://doi.org/10.1016/j.carbon.2017.08.062.

[28] J.Q. Huang, W.G. Chong, Q. Zheng, Z.L. Xu, J. Cui, S. Yao, C. Wang, J.K. Kim, Understanding the roles of activated porous carbon nanotubes as sulfur support and separator coating for lithium-sulfur batteries, Electrochim. Acta 268 (2018) 1–9, https://doi.org/10.1016/j.electacta.2018.02.096.

[29] V.A. Online, T. Jeong, Y.H. Moon, H. Chun, H.S. Kim, B.W. Cho, Y. Kim, Free standing acetylene black mesh to capture dissolved polysulfide in lithium sulfur batteries, (2013) 11107–11109. Doi: 10.1039/c3cc46358c.

[30] G. Zhou, H. Tian, Y. Jin, X. Tao, B. Liu, R. Zhang, Z. Wei, D. Zhuo, Catalytic oxidation of Li2S on the surface of metal sulfides for Li − S batteries, (2016). Doi: 10.1073/pnas.1615837114.

[31] D.S. Wu, F. Shi, G. Zhou, C. Zu, C. Liu, K. Liu, Y. Liu, J. Wang, Y. Peng, Y. Cui, Author’s accepted manuscript, Energy Storage Mater. (2018), https://doi.org/10.1016/j.ensm.2018.01.020.

[32] S. Rehman, S. Guo, Y. Hou, Rational design of Si/SiO2 @ hierarchical porous carbon spheres as efficient polysulfi de reservoirs for high-performance Li–S battery, (2016) 3167–3172. Doi: 10.1002/adma.201506111.

[33] A. Raghunandanan, P. Periasamy, P. Ragupathy, Surface-activated graphite paper for high-performance lithium-polysulfide batteries, ACS Sustain. Chem. Eng. 7 (2018) 276–284, https://doi.org/10.1021/acssuschemeng.8b03193.

[34] H.Y. Park, M.S. Kim, T.S. Bae, J. Yuan, J.S. Yu, Fabrication of binder-free pencil-trace electrode for lithium-ion battery: Simplicity and high performance, Langmuir 32 (2016) 4415–4423, https://doi.org/10.1021/acs.langmuir.5b04641.

[35] J.-Q. Huang, Q. Zhang, S.-M. Zhang, X.-F. Liu, W. Zhu, W.-Z. Qian, F. Wei, Aligned sulfur-coated carbon nanotubes with a polyethylene glycol barrier at one end for use as a high efficiency sulfur cathode, Carbon 58 (2013) 99–106.

[36] W.J. Hehre, R. Ditchfield, J.A. Pople, Self—consistent molecular orbital methods. XII. Further extensions of Gaussian—type basis sets for use in molecular orbital studies of organic molecules, J. Chem. Phys. 56 (1972) 2257–2261.

[37] J.D. Dill, J.A. Pople, Self-consistent molecular orbital methods. XV. Extended Gaussian-type basis sets for lithium, beryllium, and boron, J. Chem. Phys. 62 (1975) 2921–2923.

[38] M.M. Francl, W.J. Pietro, W.J. Hehre, J.S. Binkley, M.S. Gordon, D.J. DeFrees, J.A. Pople, Self-consistent molecular orbital methods. XXIII. A polarization-type basis set for second-row elements, J. Chem. Phys. 77 (1982) 3654–3665.

[39] A.D. Becke, Density-functional thermochemistry. III. The role of exact exchange, J. Chem. Phys. 98 (1993) 5648–5652.

[40] P.J. Stephens, F.J. Devlin, C.F. Chabalowski, M.J. Frisch, Ab Initio calculation of vibrational absorption and circular dichroism spectra using density functional force

fields, J. Phys. Chem. 98 (1994) 11623–11627.
[41] Y. Fan, Z. Niu, F. Zhang, R. Zhang, Y. Zhao, G. Lu, Suppressing the shuttle effect in lithium-sulfur batteries by a UiO-66-modified polypropylene separator, ACS Omega 4 (2019) 10328–10335.
[42] J.W. Buchanan, Observational models of graphite pencil materials, 18 (1999).
[43] C. Deng, Z. Wang, S. Wang, J. Yu, Inhibition of polysulfide diffusion in lithium-sulfur batteries: mechanism and improvement strategies, J. Mater. Chem. A 7 (2019) 12381–12413, https://doi.org/10.1039/c9ta00535h.
[44] M.W. Smith, I. Dallmeyer, T.J. Johnson, C.S. Brauer, J.S. McEwen, J.F. Espinal, M. Garcia-Perez, Structural analysis of char by Raman spectroscopy: Improving band assignments through computational calculations from first principles, 2016. Doi: 10.1016/j.carbon.2016.01.031.
[45] J. Bin Wu, M.L. Lin, X. Cong, H.N. Liu, P.H. Tan, Raman spectroscopy of graphene-based materials and its applications in related devices, Chem. Soc. Rev. 47 (2018) 1822–1873, https://doi.org/10.1039/c6cs00915h.
[46] T. Purkait, G. Singh, M. Singh, D. Kumar, R.S. Dey, Large area few-layer graphene with scalable preparation from waste biomass for high-performance supercapacitor, Sci. Rep. 7 (2017) 1–14, https://doi.org/10.1038/s41598-017-15463-w.
[47] G.S. Pappas, S. Ferrari, X. Huang, R. Bhagat, Heteroatom doped-carbon nanospheres as anodes, (2016). Doi: 10.3390/ma9010035.
[48] T.Z. Hou, X. Chen, H.J. Peng, J.Q. Huang, B.Q. Li, Q. Zhang, B. Li, Design principles for heteroatom-doped nanocarbon to achieve strong anchoring of polysulfides for lithium-sulfur batteries, Small (2016) 3283–3291, https://doi.org/10.1002/smll.201600809.
[49] R. Jayan, M.M. Islam, First-principles investigation of anchoring behavior of WS2 and WSe2 for lithium-sulfur batteries, (2020) 2–8. http://arxiv.org/abs/2001.05442.
[50] B. Marinho, M. Ghislandi, E. Tkalya, C.E. Koning, G. de With, Electrical conductivity of compacts of graphene, multi-wall carbon nanotubes, carbon black, and graphite powder, Powder Technol. 221 (2012) 351–358, https://doi.org/10.1016/j.powtec.2012.01.024.
[51] R. Scipioni, L. Stixrude, M.P. Desjarlais, Electrical conductivity of SiO2 at extreme conditions and planetary dynamos, Proc. Natl. Acad. Sci. U. S. A. 114 (2017) 9009–9013, https://doi.org/10.1073/pnas.1704762114.
[52] W.M.A. El Rouby, Crumpled graphene: preparation and applications, RSC Adv. 5 (2015) 66767–66796, https://doi.org/10.1039/c5ra10289h.
[53] J. Li, K. Yu, K. Qian, H. Cao, X. Lu, J. Sun, The situ preparation of silica nanoparticles on the surface of functionalized graphene nanoplatelets, Nanoscale Res. Lett. 9 (2014) 1–9, https://doi.org/10.1186/1556-276X-9-172.
[54] M.M. Gaikwad, M. Kakunuri, C.S. Sharma, Enhanced catalytic graphitization of resorcinol formaldehyde derived carbon xerogel to improve its anodic performance for lithium ion battery, Mater. Today Commun. 20 (2019) 100569, https://doi.org/10.1016/j.mtcomm.2019.100569.
[55] C.C. Walters, C.E. Kliewer, D.N. Awwiller, M.D. Rudnicki, Q.R. Passey, M.W. Lin, Influence of turbostratic carbon nanostructures on electrical conductivity in shales, Int. J. Coal Geol. 122 (2014) 105–109, https://doi.org/10.1016/j.coal.2013.12.015.
[56] S. Mamidi, A. Gangadharan, C.S. Sharma, Graphite coated pyrolyzed filter paper as a low-cost binder-free and freestanding anode for practical lithium-ion battery application, Electrochim. Acta 310 (2019) 222–229, https://doi.org/10.1016/j.electacta.2019.04.131.
[57] S. Li, G. Ren, M.N.F. Hoque, Z. Dong, J. Warzywoda, Z. Fan, Carbonized cellulose paper as an effective interlayer in lithium-sulfur batteries, Appl. Surf. Sci. 396 (2017) 637–643, https://doi.org/10.1016/j.apsusc.2016.10.208.
[58] L.A. Zemnukhova, A.E. Panasenko, A.P. Artem'yanov, E.A. Tsoy, Dependence of porosity of amorphous silicon dioxide prepared from rice straw on plant variety, BioResources 10 (2015) 3713–3723, https://doi.org/10.15376/biores.10.2.3713-3723.
[59] T.N. Tran, T.V.A. Pham, M.L.P. Le, T.P.T. Nguyen, V.M. Tran, Synthesis of amorphous silica and sulfonic acid functionalized silica used as reinforced phase for polymer electrolyte membrane, Adv. Nat. Sci.: Nanosci. Nanotechnol. 4 (2013), https://doi.org/10.1088/2043-6262/4/4/045007.
[60] J.V.G. Tinio, K.T. Simfroso, A.D.M.V. Peguit, R.T. Candidato, Influence of OH- ion concentration on the surface morphology of znO-siO2 nanostructure, J. Nanotechnol. 2015 (2015), https://doi.org/10.1155/2015/686021.
[61] X. Qiu, Q. Hua, L. Zheng, Z. Dai, Study of the discharge/charge process of lithium-sulfur batteries by electrochemical impedance spectroscopy, RSC Adv. 10 (2020) 5283–5293, https://doi.org/10.1039/c9ra10527a.
[62] Y.V. Mikhaylik, J.R. Akridge, Polysulfide shuttle study in the Li/S battery system, J. Electrochem. Soc. 151 (2004) A1969, https://doi.org/10.1149/1.1806394.
[63] K. Yang, L. Zhong, R. Guan, M. Xiao, D. Han, S. Wang, Y. Meng, Carbon felt interlayer derived from rice paper and its synergistic encapsulation of polysulfides for lithium-sulfur batteries, Appl. Surf. Sci. 441 (2018) 914–922, https://doi.org/10.1016/j.apsusc.2018.02.108.
[64] Y. Lu, S. Gu, J. Guo, K. Rui, C. Chen, S. Zhang, J. Jin, J. Yang, Z. Wen, Sulfonic groups originated dual-functional interlayer for high performance lithium − sulfur battery, (2017). Doi: 10.1021/acsami.7b02142.
[65] H. Tang, S. Yao, S. Xue, M. Liu, L. Chen, M. Jing, X. Shen, T. Li, K. Xiao, S. Qin, In-situ synthesis of carbon@Ti4O7 non-woven fabric as a multi-functional interlayer for excellent lithium-sulfur battery, Electrochim. Acta 263 (2018) 158–167, https://doi.org/10.1016/j.electacta.2018.01.066.
[66] F. Wu, Y. Ye, R. Chen, J. Qian, T. Zhao, L. Li, W. Li, Systematic effect for an ultralong cycle lithium-sulfur battery, Nano Lett. 15 (2015) 7431–7439, https://doi.org/10.1021/acs.nanolett.5b02864.
[67] F. Wu, J. Qian, R. Chen, Y. Ye, Z. Sun, Y. Xing, L. Li, Light-weight functional layer on a separator as a polysulfide immobilizer to enhance cycling stability for lithium-sulfur batteries, J. Mater. Chem. A 4 (2016) 17033–17041, https://doi.org/10.1039/c6ta06516c.
[68] C. Lin, W. Zhang, L. Wang, Z. Wang, W. Zhao, W. Duan, Z. Zhao, B. Liu, J. Jin, A few-layered Ti3C2 nanosheet/glass fiber composite separator as a lithium polysulphide reservoir for high-performance lithium-sulfur batteries, J. Mater. Chem. A 4 (2016) 5993–5998, https://doi.org/10.1039/c5ta10307j.
[69] J. Liu, L. Yuan, K. Yuan, Z. Li, Z. Hao, J. Xiang, Y. Huang, SnO2 as a high-efficiency polysulfide trap in lithium-sulfur batteries, Nanoscale 8 (2016) 13638–13645, https://doi.org/10.1039/c6nr02345b.